

# DFT Characterization of Key Intermediates in Thiols Oxidation

## Catalyzed by Amavadin. Supplementary Information.

10/05/2011

Luca Bertini, Valentina Barbieri, Piercarlo Fantucci, Luca De Gioia, Giuseppe Zampella\*

Department of Biotechnology and Biosciences, Università degli Studi di Milano-Bicocca, Piazza della Scienza, 2; 20126

Milan - Italy

<sup>†</sup>To whom correspondence should be addressed: [giuseppe.zampella@unimib.it](mailto:giuseppe.zampella@unimib.it)

### 1. Optimized geometry parameters as a function of the DFT functional. B-P86 vs B3-LYP.

In order to evaluate the effects of the different DFT functionals on the optimized bond distance values, we have optimized the  $[V(\text{hidpa})_2]^{2-}$  and  $[V(\text{hidpa})_2]^-$  using the hybrid at B-3LYP functional adopting the same TZVP basis set.

$[V(\text{hidpa})_2]^{2-}$	B-P86	B3-LYP	$\Delta$	XRD	$\Delta$ B-P86	$\Delta$ B3-LYP
V-NO	2.045	2.042	0.003	1.999	0.046	0.043
	2.045	2.042	0.003	1.982	0.063	0.06
V-ON	1.985	1.973	0.012	1.94	0.045	0.033
	1.988	1.973	0.015	1.956	0.032	0.017
V-O	2.085	2.083	0.002	2.028	0.057	0.055
	2.112	2.11	0.002	2.07	0.042	0.04
	2.085	2.082	0.003	2.028	0.057	0.054
	2.111	2.11	0.001	2.042	0.069	0.068
$\langle \cdot \rangle \pm \sigma$			0.005 $\pm$ 0.005		0.051 $\pm$ 0.012	0.046 $\pm$ 0.016
$[V(\text{hidpa})_2]^-$	B-P86	B3-LYP	$\Delta$	XRD	$\Delta$ B-P86	$\Delta$ B3-LYP
V-NO	2.043	2.035	0.008	1.999	0.044	0.036
	2.043	2.034	0.009	2.018	0.025	0.016
V-ON	1.958	1.947	0.011	1.94	0.018	0.007
	1.956	1.946	0.01	1.923	0.033	0.023
V-O	1.974	1.962	0.012	1.972	0.002	0.01
	2.043	2.023	0.02	1.993	0.05	0.03
	1.973	1.961	0.012	1.959	0.014	0.002
	2.043	2.023	0.02	1.997	0.046	0.026
$\langle \cdot \rangle \pm \sigma$			0.013 $\pm$ 0.005		0.029 $\pm$ 0.017	0.018 $\pm$ 0.012

Considering the eight bond distances that characterized the  $\{VO_6N_2\}$  coordination, for  $[V(\text{hidpa})_2]^{2-}$  the average absolute B-P86-B3-LYP difference is  $0.005\text{\AA}\pm 0.005\text{\AA}$ , where the highest difference is found for the two V-ON distances that result  $0.012\text{\AA}$  and  $0.015\text{\AA}$  shorter at B3-LYP level with respect to B-P86. Regarding  $[V(\text{hidpa})_2]^-$ , the differences among B3-LYP and B-P86 optimized distances are slightly higher (the same average difference is  $0.013\text{\AA}\pm 0.005\text{\AA}$ ).

The comparisons with the XRD distances found in literature are not completely fair, since we do not include the counterion ( $\text{Ca}^{2+}$  for  $[V(\text{hidpa})_2]^{2-}$ ,  $\text{PPh}_4^+$  for  $[V(\text{hidpa})_2]^-$ ) in the investigated systems. The effect of counterions on the crystal structure is the lowering of symmetry of the complex, while, at computational level without counterions, the optimized geometry structures result close to  $C_2$  symmetry. B3-LYP bond distances result in a slightly better agreement with XRD values (average |experimental-theoretical|:  $[V(\text{hidpa})_2]^{2-}$   $0.051\pm 0.012$  (B-P86),  $0.046\pm 0.016$  (B3-LYP);  $[V(\text{hidpa})_2]^-$ :  $0.029\pm 0.017$  (B-P86),  $0.019\pm 0.011$  (B3-LYP)). However, these values overlap within one standard deviation, and therefore we can conclude that the quality of the optimized geometry parameters using these two DFT functionals is very similar.

## 2. TDDFT computed electronic spectrum for $[\text{V}(\text{hidpa})_2]^{2-}$ and $[\text{V}(\text{hidpa})_2]^-$ .

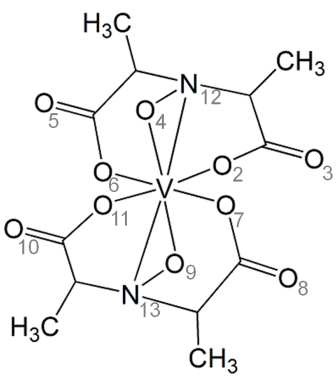
In quality, the TDDFT computation of the electronic spectra of transition metal complexes strongly depends on the DFT functional adopted, in particular when charge transfer bands are considered,<sup>1</sup> essentially due to the fact virtual MO energies of the DFT wave-function used to compute the TDDFT spectrum are not directly optimized in mono-determinant methods, as in the case of DFT. For this reason, the discrepancy between computed and measured excitation energies can be in the range of the tenths of nm. The B-P86 functional has been adopted, although it is known that this is not the best choice to reproduce excitation energies for MLCT bands. However, the assignment of the bands are generally reliable.

The  $[\text{V}(\text{hidpa})_2]^{2-}$  and  $[\text{V}(\text{hidpa})_2]^-$  TDDFT/B-P86 UV-Vis spectra computed up to 300 nm are reported below.

$[\text{V}(\text{hidpa})_2]^{2-}$					
<i>N</i>	<i>nm</i>	<i>F</i>	<i>a</i> → <i>i</i>	<i>Exp</i>	
1	816.7 (+57.6)	$1 \cdot 10^{-4}$	104a(α)→105a(α)	759.1	
2	760.6 (+62.8)	$1 \cdot 10^{-4}$	104a(α)→106a(α)	697.8	
3	634.1 (+71.0)	$2 \cdot 10^{-4}$	104a(α)→108a(α)	563.1	
4	628.6	$2 \cdot 10^{-4}$	104a(α)→107a(α)		
5	435.9	$6 \cdot 10^{-3}$	104a(α)→109a(α) (51.4) 104a(α)→110a(α) (49.8)		
6	434.6	$1 \cdot 10^{-3}$	104a(α)→110a(α) (51.4) 104a(α)→109a(α) (49.8)		
7	385.2	$5 \cdot 10^{-3}$	104a(α)→111a(α)		
8	380.8 (+63.6)	$7 \cdot 10^{-3}$	104a(α)→112a(α)	444.4	
9	365.2	$9 \cdot 10^{-5}$	101a(α)→105a(α) 101a(α)→112a(α)		
10	357.1 (+87.3)	$7 \cdot 10^{-3}$	103a(α)→105a(α)	444.4	
$[\text{V}(\text{hidpa})_2]^-$					
1	650.6	$1 \cdot 10^{-5}$	103a→104a		
2	647.6	$1 \cdot 10^{-4}$	102a→104a		
3	562.3	$6 \cdot 10^{-4}$	101a→104a		
4	557.6	$1 \cdot 10^{-3}$	100a→104a		
5	495.4	$1 \cdot 10^{-3}$	99a→104a (79.1) 96a→104a (17.2)		
6	491.0	$7 \cdot 10^{-5}$	98a→104a		
7	484.0	$3 \cdot 10^{-3}$	96a→104a (79.9) 99a→104a (16.0)		
8	479.8	$3 \cdot 10^{-3}$	97a→104a (88.2) 98a→104a (7.8)		
9	436.3	$1 \cdot 10^{-2}$	95a→104a		

We first consider the discussion of the d-d part of the  $[\text{V}(\text{hidpa})_2]^{2-}$  spectrum in the visible region between 600-900 nm. In Table are reported the computed transition energies in the range up to 400 nm with the corresponding oscillation (*f*) strengths and leading one-electron excitations (*a*→*i*). The *d-d* portion of the  $[\text{V}(\text{hidpa})_2]^{2-}$  is reasonably reproduced by TDDFT, and the computed excitation energies result lower on average by 64 nm with respect to the corresponding experimental values. The *d-d*

spectrum is characterized by four transitions of HOMO→LUMO+n (n=0,3) type. According to the analysis of the prevalent FMOs orbital composition, the *d*-orbital splitting due to the particular V<sup>IV</sup> coordination in amavadin is  $d_{x^2-y^2}^{(1)} d_{yz} d_{xz} d_{yz} d_{z^2}$ , which is in agreement with previous results. Below are reported the MO Mulliken populations of the FMOs involved in the low-energy electronic excitations (in bold the highest atomic MO population, the label of the atom are reported according to the schema below):

		103( $\alpha$ )	104( $\alpha$ )	105( $\alpha$ )	106( $\alpha$ )	107( $\alpha$ )	108( $\alpha$ )
		HOMO-1( $\alpha$ )	SOMO( $\alpha$ )	LUMO( $\alpha$ )	LUMO+1( $\alpha$ )	LUMO+2( $\alpha$ )	LUMO+3( $\alpha$ )
	V 1	0.03	<b>0.8</b>	<b>0.66</b>	<b>0.59</b>	<b>0.71</b>	<b>0.79</b>
	O 2	0.01	0.02	0.02	0.01	0.	0.04
	O 3	0.05	0.01	0.	0.	0.	0.
	O 4	0.02	0.01	0.03	0.07	0.09	0.
	O 5	<b>0.26</b>	0.01	0.	0.	0.	0.
	O 6	0.03	0.02	0.	0.01	0.03	0.03
	O 7	0.03	0.02	0.	0.01	0.03	0.03
	O 8	<b>0.26</b>	0.01	0.	0.	0.	0.
	O 9	0.02	0.01	0.03	0.08	0.09	0.
	O 10	0.05	0.01	0.	0.	0.	0.
	O 11	0.01	0.02	0.02	0.01	0.	0.04
	N 12	0.01	0.	0.08	0.06	0.	0.
	N 13	0.01	0.	0.08	0.06	0.	0.

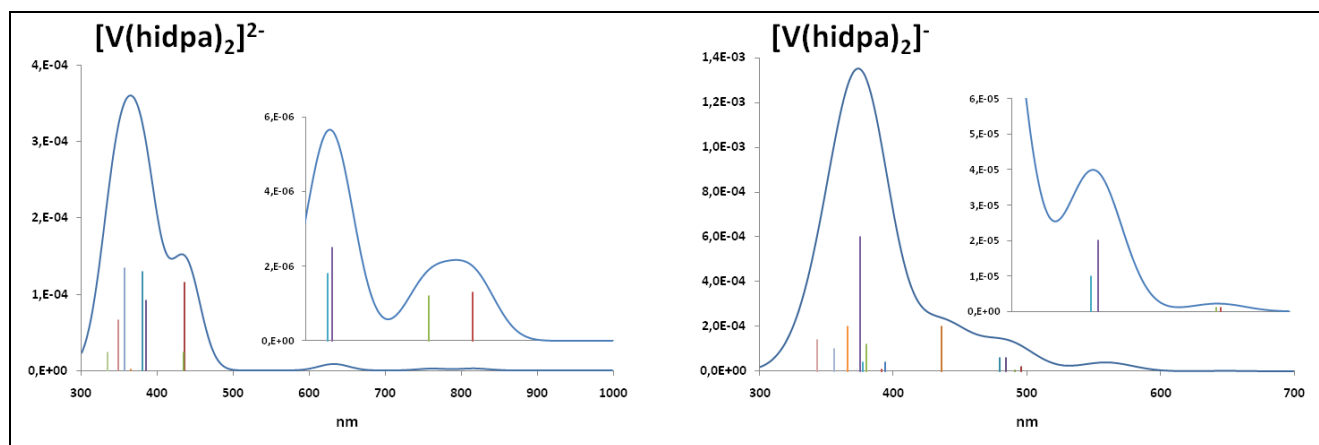
Below we report the *d*-orbital Mulliken populations for the same MOs considered above (in bold the highest population value).

MO	$z^2$	$xz$	$yz$	$xy$	$x^2-y^2$
104( $\alpha$ )	0.02	0.03	0.29	0.11	<b>0.35</b>
105( $\alpha$ )	0.01	<b>0.41</b>	0.00	0.12	0.12
106( $\alpha$ )	<b>0.30</b>	0.03	0.08	0.14	0.05
107( $\alpha$ )	0.22	0.04	<b>0.35</b>	0.02	0.07
108( $\alpha$ )	0.10	0.21	0.01	<b>0.34</b>	0.12

According to the results presented in the two tables above, the low-energy excitations has a small MLCT character, mainly of V→NO type. The values of the *d*-orbital populations testify to the d-d character of these bands. It is interesting that the *d*<sup>1</sup> electron results delocalized between the  $x^2-y^2$  and  $yz$  *d*-orbitals.

Finally, the measured 444.4 nm CT band can be assigned to the two most intense transitions at 357.1 nm and 380.8 nm with HOMO-1( $\alpha$ )→LUMO+1( $\alpha$ ) and SOMO( $\alpha$ )→LUMO+7( $\alpha$ ) main mono-electronic excitations, respectively. The analysis of the MO involved in these band reveals their LMCT character with the oxygen atoms of the carboxylate groups.

The spectrum of the oxidized form is not known experimentally. At computational level, all the transition considered are of HOMO-n→LUMO type, where the LUMO is the empty SOMO of V<sup>IV</sup> form. Because of the *d*<sup>0</sup> electronic configuration of the V atom, essentially all the excitations are essentially of LMCT type.



TDDFT B-P86/TZVP computed electronic spectra for  $[\text{V}(\text{hidpa})_2]^{2-}$  (left) and  $[\text{V}(\text{hidpa})_2]^-$  (right). In the inset are reported the magnificated d-d spectra in the visible region.  $[\text{V}(\text{hidpa})_2]^{2-}$  experimental d-d transition in water are  $13175 \text{ cm}^{-1}$  (759,1 nm,  $\epsilon = 22.1 \text{ dm}^3 \text{ mol}^{-1} \text{ cm}^{-1}$ );  $14330 \text{ cm}^{-1}$  (697.8 nm,  $\epsilon = 21.6 \text{ dm}^3 \text{ mol}^{-1} \text{ cm}^{-1}$ );  $17760 \text{ cm}^{-1}$  (563.1 nm,  $\epsilon = 23.4 \text{ dm}^3 \text{ mol}^{-1} \text{ cm}^{-1}$ ). Charge Transfer (CT) bands at  $22500 \text{ cm}^{-1}$  (444.4 nm). (Armstrong and co-workers<sup>2</sup>)

<sup>1</sup> Adamo, C.; Scuseria, G.; Barone, V. *J. Chem. Phys.* **1999**, *111*, 2889.

<sup>2</sup> E. M. Armstrong, D. Collison, R. J. Deeth, C. D. Garnera, *J. Chem. soc. Dalton Trans.* **1995**, 191.